Electrochimica Acta 178 (2015) 65–73

Contents lists available at ScienceDirect

Electrochimica Acta

journal homepage: www.elsevier.com/locate/electacta

Porous microspherical silicon composite anode material for lithium ion battery

Yitian Bie[a,1], Jinglu Yu[a,1], Jun Yang[a,*], Wei Lu[b], Yanna Nuli[a], Jiulin Wang[a]

[a] Shanghai Electrochemical Energy Devices Research Center, School of Chemistry and Chemical Engineering, Shanghai Jiao Tong University, Shanghai, 200240, China

[b] Department of Chemical Engineering, University of Michigan, Ann Arbor, MI 48109, USA

ARTICLE INFO

Article history:
Received 29 March 2015
Received in revised form 14 July 2015
Accepted 30 July 2015
Available online 1 August 2015

Keywords:
Silicon
Carbon nanotubes
Spray drying
Lithium-ion battery

ABSTRACT

Nano/micro-structured Si/CNT/C and Si-Cu/CNT/C microspheres are prepared by two simple steps of spray drying and carbonization, which are efficient and easy to scale up. In the Si/CNT/C composites, silicon particles (about 50–200 nm) are covered by a layer of carbon formed by pyrolysis of phenol-formaldenhyde resin (PF), which, in turn, connects with the three-dimensional multiwall carbon nanotubes (MWCNTs) conductive network. Numerous open pores, which could buffer volume expansion of silicon and improve the electrode kinetics, are engendered in the microspheres due to the rapid evaporation of solvent and unfoldment of flexible MWCNTs. Moreover, introduction of small amount of copper (5 wt.%) into the microspheres as Cu_3Si phase reinforces the mechanical stability and improves the electronic conductivity. The favorable Si/CNT/C composite structure leads to significantly improved cycling stability and rate performance (ca. 1250 mA h g^{-1} at 5 A g^{-1}) compared to pristine Si particles. Addition of copper further enhances the capacity retention to 91.2% after 80 cycles.

1. Introduction

As the growing demands for the next-generation lithium ion batteries with increased energy and power density used in portable electronic devices and electric vehicles, silicon has attracted extensive attention owning to its high theoretical capacity ($Li_{22}Si_5$, 4200 mAh g^{-1}) and moderate operating voltage (0.4 V vs Li/Li^+) [1–3]. However, silicon based electrodes often show poor cycle performance because of its low conductivity and the dramatic volume change during repeated lithiation/delithiation process, which leads to electrode pulverization and instability of the solid-electrolyte interphase (SEI) [4–7]. Many methods have been developed to overcome these problems, such as porous Si structure, nanosize Si and Si/C composite [8–12]. Ge Mingyuan et al. [8] reported porous silicon nanowires synthesized by direct etching of boron-doped silicon wafers. The large pore size and high porosity of porous silicon contribute to the structural stability during lithium ion intercalation, resulting in high capacity and long cycle retention. Using alginate as binder, the electrode exhibited the reversible capacity of more than 2000 mA h g^{-1} at current rates of 2 A g^{-1} even after 250 cycles. Hysesun Kim et al. [9] prepared mesoporous Si@carbon core-shell nanowires using a SBA-15 template. The composite electrode showed good cycle performance with 87% capacity retention after 80 cycles.

Moreover, studies [13–18] show that a mixed-conduction carbon phase, such as incorporation of graphite, CNT or grahene, can improve the electronic conductivity, thus contributing to better cycle performance and rate performance. In particular, MWCNTs [14,19] are considered to be benefical for stablizing the conducting structure and enhancing mechanical properties. It was reported that the introduction of MWCNT for silicon electrode could increase the cycling performance [20]. Dae Soo Jung [10]. reported a spray drying process to synthesize porous Si/C composite particles. The porous structure arose mainly from HF etching of SiO_2. The composite electrodes exhibit 91% capacity retention after 150 cycles and 1956 mA h g^{-1} at 0.05 C. Our group proposed [18] a hierarchical microstructured pSi/CNT/C composite prepared from nano-SiO_2 as silicon precursor via a combination of spray drying and magnesiothermic reduction, followed by a nano-layer carbon coating by chemical vapor deposition. Carbon coated silicon nano-particles bonded MWCNT uniformly to form the second particles. This composite presented specific capacity of ca. 2100 mA h g^{-1} at 1 A $g^{-1}$and 95.5% capacity retention after 100 cycles.

Although the above Si based materials show excellent electrochemical performance, most of them are difficult for practical application due to the complicated preparation routes,

* Corresponding author.
E-mail address: yangj723@sjtu.edu.cn (J. Yang).
[1] These authors contributed equally.

http://dx.doi.org/10.1016/j.electacta.2015.07.173
0013-4686/

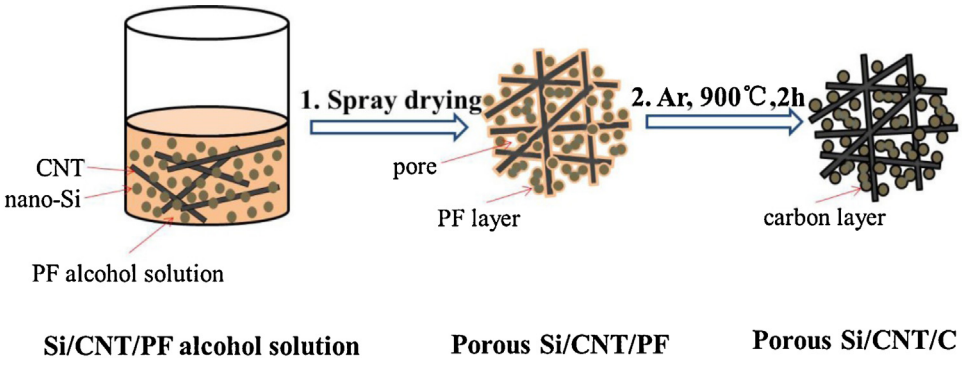

Scheme 1. Schematic for the synthesis route of the spray Si composite.

expensive precursors like SBA-15 template or plagued waste water treatment. Spray drying(SD) method has been widely used for powder preparation and nanoparticle encapsulation in the chemical and food industries owing to its low cost, simple apparatus and easy to scale up [21]. Here, we directly use commercialized nano-Si powder and adopt a two-step procedure consisting of spray drying and carbonization to produce porous Si/CNT/C spheres. Moreover, in view of that Cu and Cu-Si alloy have a low contact resistance and a high mechanical tolerance to volume change [22,23], we add copper into the composite to reinforce the structural stability. The composite electrodes show superior cycle performance and excellent rate capability.

2. Experimental

2.1. Material preparation

2.1.1. Preparation of spray Si

Firstly, 0.73 g nano-Si (particle size of 50-200 nm, Alfa-Aesar), 0.11 g MWCNT (OD > 50 nm, length of 10–30 μm, purity > 95%, Chengdu Organic Chemicals Co., Ltd., China) and 0.37 g PF (Shandong Shenquan Group, China) were dispersed in 150 mL absolute ethanol. The mixture was stirred for 4 h and sonicated for 1 hour at room temperature. Secondly, the mixture was spray-dried (inlet temperature: 170 °C; outlet temperature: 100 °C) to form PF-wrapped nano-Si and MWCNT composite microparticles (Si/CNT/PF). The obtained precursor was then heated to 900 °C at a speed of 5 °C min^{-1} and this temperature was maintained for 2 h in Ar atmosphere to convert PF to amorphous carbon. The whole preparation route is illustrated in Scheme 1. According to the carbonization rate (57%) of PF, the weight ratio of Si:CNT:C in the composite is 69:10:21. The prepared porous Si/CNT/C particles are designated as spray Si.

2.1.2. Preparation of spray Si-Cu

The given amount of the above-mentioned nano-Si, MWCNT and PF, plus Cu nano-powder (10-30 nm, Aladdin), were dispersed in absolute ethanol. After the same procedure in Scheme 1, the Si-Cu/CNT/C composite with a weight ratio of 65:10:20:5 for Si:CNT:C:Cu was obtained, which is described as spray Si-Cu. The tapping

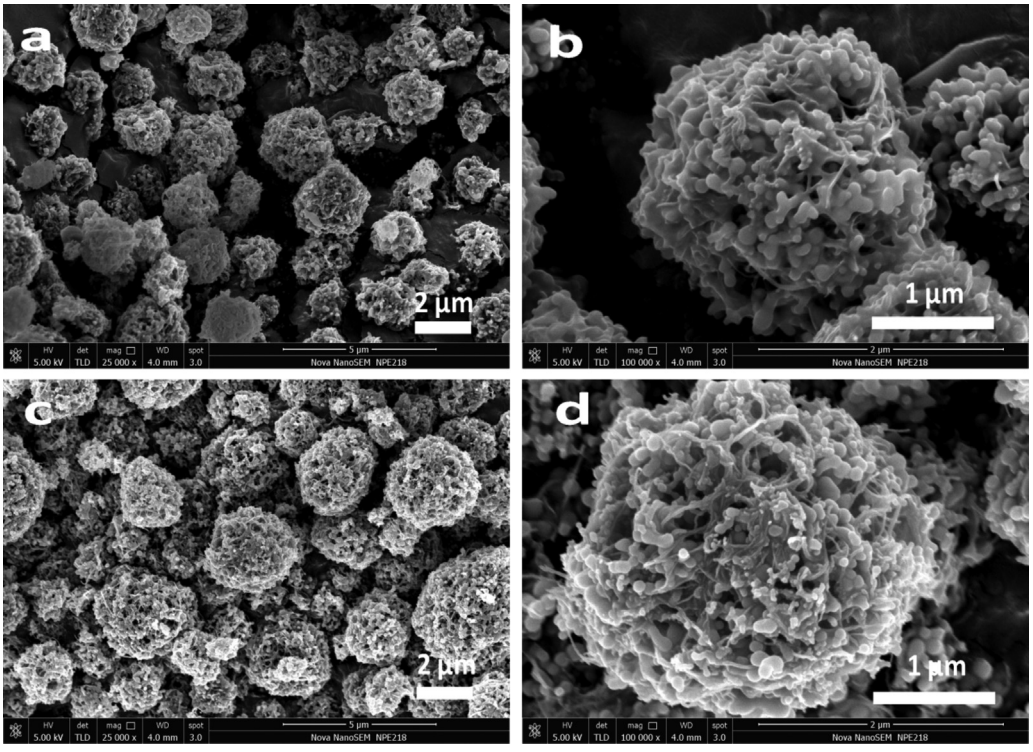

Fig. 1. SEM images of (a, b) Si/CNT/PF after spray drying, (c, d) spray Si after calcination at 900 °C for 2 h in Ar atmosphere.

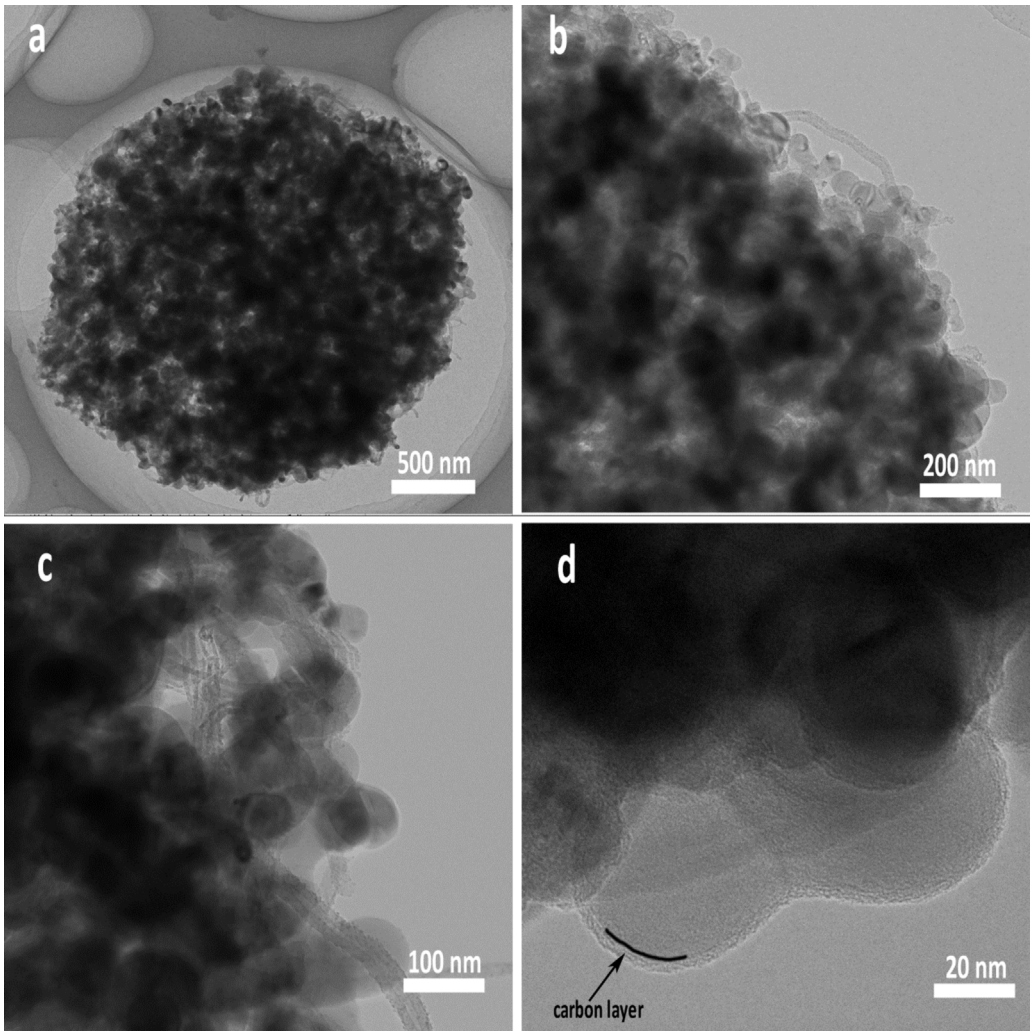

Fig. 2. TEM images of spray Si from low to high magnifications.

densities of spray Si and spray Si-Cu are ca. 0.48 and 0.54 g cm^{-3}, respectively

For comparison, nano-Si powder was directly used for the electrode preparation and the electrode samples were designated as nano-Si.

2.2. Morphology and structure characterization

The morphologies and microstructures of the samples were investigated by a FEI Nova SEM 230 ultra-high resolution FESEM and a JEM-2100F TEM (JEOL Ltd, Japan). The phase structures of the composites were determined by X-ray diffraction (XRD) measurements using a Rigaku D/MAX-220-PC X-ray diffractometer at 40 kV and 30 mA with a Cu Kα radiation source. The specific surface area and pore size distribution were determined by the results of the nitrogen adsorption/desorption measurements using an ASAP 2020 accelerated surface area and porosimetry (Micrometrics Inc., USA).

2.3. Cells assembling and electrochemical tests

The electrochemical performance of the as-prepared composites was evaluated using two electrode coin-type cells. The working electrodes were prepared by pasting a mixture of active material, Super P conductive carbon black (40 nm, Timical), and styrene butadiene rubber/sodium carboxymethyl cellulose (SBR/SCMC, 3:5 by weight, resolved in distilled water) as binder at a weight ratio of 60:20:20. After coating the mixture onto Cu foil, the electrodes were dried, cut to Φ12 mm disks, pressed at 3 MPa, and finally dried at 60 °C in vacuum for 4 h. The CR2016 coin cells were assembled in an argon-filled glove box (MB-10 compact, MBraun) using 1 M $LiPF_6$ in dimethyl carbonate (DMC) and ethylene carbonate (EC) mixed solvent of 1:1 by volume, including 10 vol. % fluoroethylene carbonate (FEC) as electrolyte, ENTEK ET20-26 membrane as separator, and lithium metal as counter electrode. The cycling performance was evaluated on a LAND battery test system (CT2007A, Wuhan Jinnuo Electronics, Ltd.) at 25 °C with constant current densities. The cut-off voltage was 0.01 V versus Li^+/Li for discharge (Li insertion) and 1.2 V versus Li^+/Li for charge (Li extraction). The specific capacity was calculated on the basis of the weight of the composites. The mass loading of active materials (spray Si, spray Si-Cu, or nano-Si) in the electrodes is ca. 0.5 mg cm^{-2}. The impedances of cells were measured by Metrohm Autolab PGSTAT302N after charging to 1.2 V in the frequency range of 10 kHz to 0.1 Hz. To test the electronic conductivities of Si/CNT/C and Si-Cu/CNT/C, the composites were pressed into thin Φ12 mm

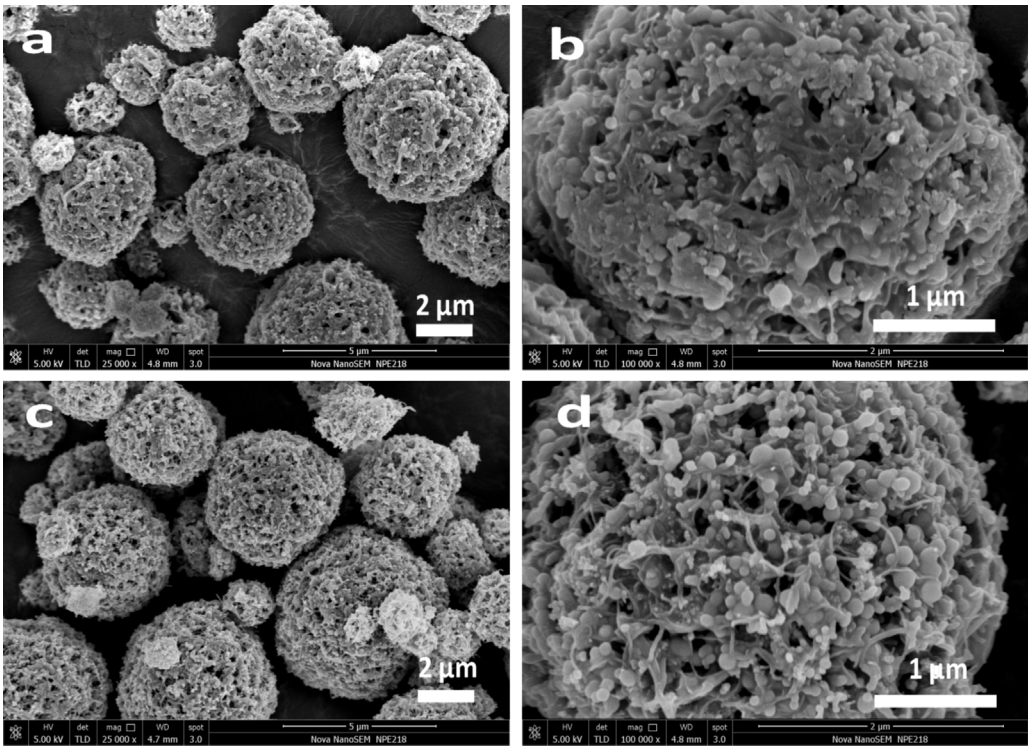

Fig. 3. SEM images of (a, b) Si/CNT/Cu/PF after spray drying, (c, d) spray Si-Cu after calcination at 900 °C for 2 h in Ar atmosphere.

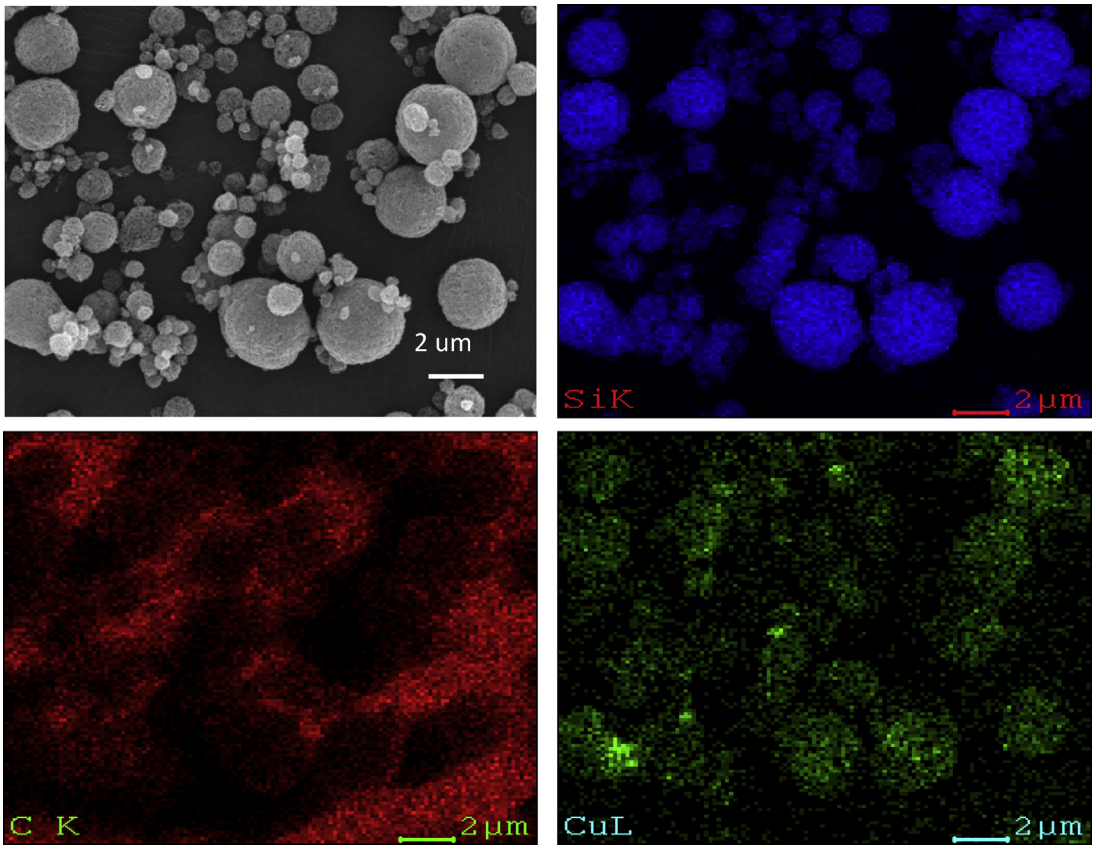

Fig. 4. SEM element mapping of spray Si-Cu composite.

wafers under the pressure of 10 MPa for 30 s. Then the electronic conductivities of the samples were measured by a 4-Point Probes Resistivity Measurement System (RTS-8, 4PROBES TECH).

3. Results and discussion

3.1. Morphology and structure analysis

Fig. 1 shows the SEM images of the samples after spray drying and carbonization in Scheme 1. Spherical Si/CNT/PF particles of a size about 3-7 μm with numerous pores were obtained after spray drying, in which silicon particles, MWCNTs and amorphous PF are uniformly distributed and connected together (Fig. 1a-b). After carbonization, the structure of microspheres is maintained and pores become larger and more obvious due to the transformation of PF to carbon (Fig. 1c-d). In order to understand the internal structure of the microspheres, TEM tests were conducted. Pores are also observed in the interior microspheres from Fig. 2a. These pores provide space for the expansion of silicon during lithium insertion and suppress the volume effect [24]. Flexible MWCNTs twist together to form the framework of microspheres and provide good mechanical properties for enduring the large volume change of silicon particles (Fig. 2b-c). Silicon particles (about 50-200 nm) are covered by a carbon layer (ca. 4 nm) formed by pyrolysis of PF (Fig. 2d), which connects with MWCNTs to constitute the three-dimensional conductive network. Hence, the firm electric contact of silicon can be ensured to a large extent.

To further improve the mechanical properties, copper nanoparticles were added in the first step in Scheme 1. As shown in Fig. 3, no obvious change on the particle morphology is observed after the addition of copper nanoparticles. Similarly, lots of pores were engendered because of rapid evaporation of solvent and unfoldment of flexible MWCNTs. According to the results of SEM element mapping in Fig. 4, copper and silicon are uniformly distributed in the microsphere. In addition, the pore structure and three-dimensional conductive network of spray Si-Cu are confirmed by TEM images in Fig. 5a-c. The enlarged TEM image of Fig. 5d shows a particle with different lattice fringes. The lattice spacing of Si (111) is 3.1 Å and the lattice spacing of 2.0 Å should correspond to Cu_3Si (300). This indicates that these two phases coexist in one particle and copper element in the microsphere exists in the form of Cu_3Si alloy. According to the result of four probe tester, the electronic conductivities of spray Si and spray Si-Cu composites are $4.03 \times 10^{-4}\,S\,cm^{-1}$ and $2.57 \times 10^{-3}\,S\,cm^{-1}$, respectively. Since Cu_3Si has a low contact resistance, high electrical conductivity and a high mechanical tolerance to volume change, its nano-dispersion in the porous spheres can improve the electrical conductivity and structural stability for lithium insertion.

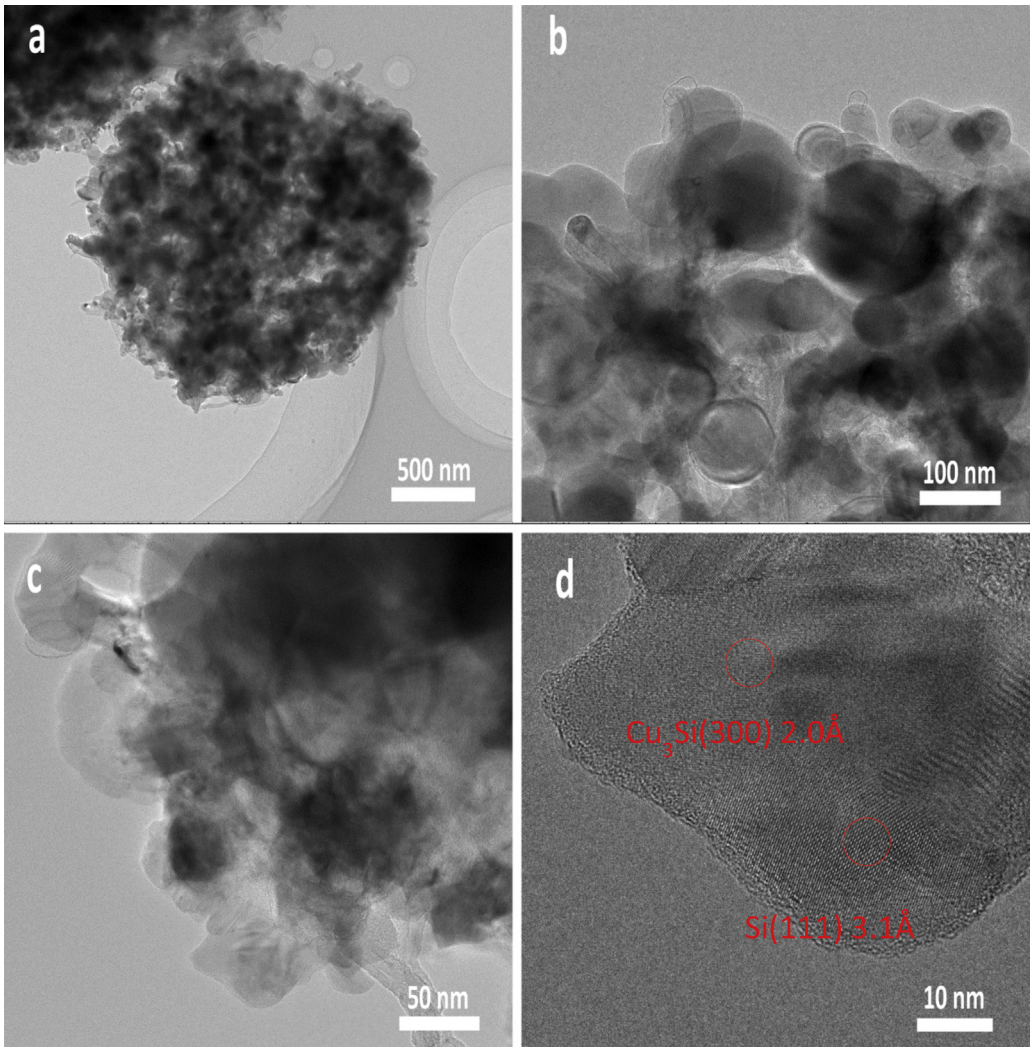

Fig. 5. TEM images of spray Si-Cu composite from low to high magnifications.

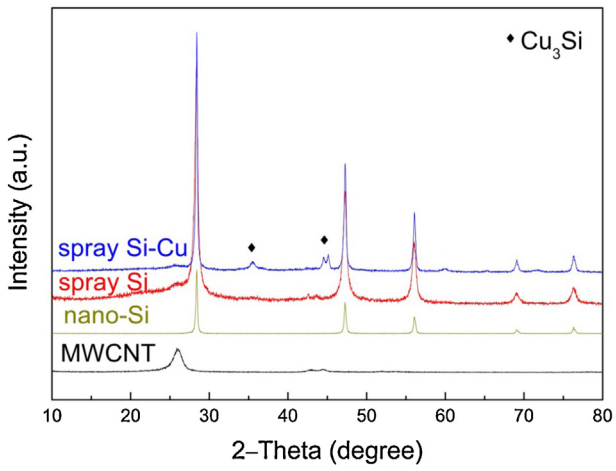

Fig. 6. XRD patterns of different samples.

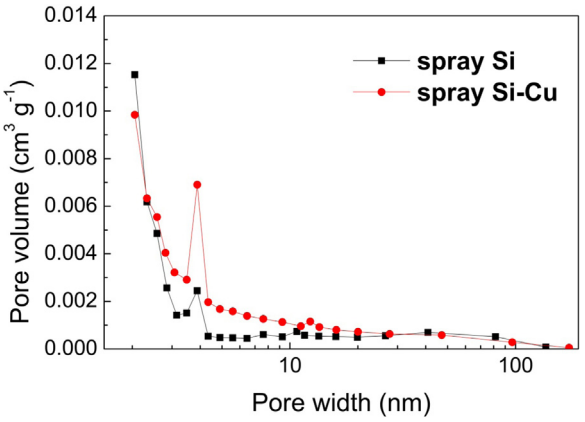

Fig. 7. Pore-size distribution plots of spray Si and spray Si-Cu.

In addition, Cu_3Si is inactive to lithium and will not experience volume change during the lithiation/delithiation process, which is favorable for the stablility of the electrode [25].

The phase structures of the composites were further checked by XRD. As shown in Fig. 6, except diffraction peaks of crystalline silicon and MWCNT, no other peaks can be observed for spray Si, indicating that no side reaction occurred during the high temperature process. Carbon does not show detectable peaks due to the amorphous or poorly crystalline structure and its minor amount. For spray Si-Cu, several weak peaks correspond to Cu_3Si phase and no XRD response of Cu can be observed. It can be concluded that copper and silicon reacted to form Cu_3Si alloy during high temperature carbonization. This result is in accord with TEM image in Fig. 5d. The porous structure of the composites were characterized by Brunaure-Emmett-Teller(BET) tests. The main pore parameters of the composites are listed in Table. 1. The specific surface areas of spray Si and spray Si-Cu are 117.69 and 109.57 $m^2 g^{-1}$ respectively. Noticeably, the pore volume increases from 0.152 to 0.176 $m^2 g^{-1}$ after addition of Cu nanoparticles, which is favorable for buffering expansion of silicon during lithium insertion. The curve trends of pore-size distribution plots in Fig. 7 rise within less than 2 nm, corresponding to micropores in amorphous carbon. The mean pore distribution for spray Si and spray Cu both lie in ca. 3.8 nm. Besides the nanopores from BET analysis, there are lots of big pores beyond 100 nm, which are observable from SEM.

3.2. Electrochemical performance

Fig. 8a shows the cycle performance of spray Si-Cu, spray Si and nano-Si in the voltage range of 0.01-1.2 V (vs. Li^+/Li). The nano-Si electrode decayed rapidly and retained less than 935 mA h g^{-1} after 80 cycles at current rate of 0.3 A g^{-1} even though it presented high initial capacity of 3279 mA h g^{-1}. It is supposed that the absence of secondary particles leads to contact loss with super p, resulting in the inferior cycling performance of Si nanoparticles [10]. In contrast, the spray Si electrode exhibited a good cycle performance with the initial capacity of 2578 mA h g^{-1} and the reversible capacity of 1866 mA h g^{-1} after 80 cycles. The porous microsphere structure with three-dimensional conductive network proves effective for stable cycling of the electrode. Furthermore, the spray Si-Cu electrode showed excellent cycleability with capacity retention of 91.2% after 80 cycles compared to the 3rd cycle (under the same current rate). It should be mentioned that the remarkable difference in the cycle stability for both the samples has little relationship to the slight distinction in their silicon contents. Even decreasing the Si content of Si/CNT/C sample to 54%, we find that its cycling trend is still similar to the existing spray Si. The superior cycle performance of spray Si-Cu can be attributed to the improvement in mechanical strength of the porous spheres by means of reinforcement of Cu_3Si alloy, which can better endure the volume change of silicon. However, the formation of inert Cu_3Si alloy consumes a portion of silicon [25], leading to the relatively low cycle capacity near 1500 mA h g^{-1}. The first cycle coulombic efficiency for nano-Si, spray Si and spray Si-Cu were 85.2%, 80.8% and 78.2%, respectively. The relatively low efficiency for the porous composites may be mainly due to their larger specific surface area, which consumes more charge for SEI formation. In the 4th cycle, both spray Si and spray Si-Cu electrodes achieved the coulombic efficiency of 98%. However, the efficiency of nano-Si electrode reached 98% in the 16th cycle and declined after 50 cycles. The voltage profiles of three electrodes are shown in Fig. 8c. With the progressive cycle number, the voltage polarization of nano-Si electrode is rapidly enhanced. In comparison, the charge and discharge curves of spray Si and spray Si-Cu change slightly during cycling. Especially for spray Si-Cu electrode, its discharge curves almost overlap at current rate of 0.3 A g^{-1}, indicating its high electrochemical reversibility.

Fig. 8b compares the rate capability of nano-Si, spray Si and spray Si-Cu. The nano-Si electrode exhibits a higher capacity than others at the first few cycles with a low current rate due to the higher content of active material. However, its capacity decreased rapidly with increasing current rate. The spray Si shows superior rate performance with the specific capacity of 1248 mA h g^{-1} at a

Table 1
Surface area and pore volume of spray Si and spray Si-Cu.

	BET surface area ($m^2 g^{-1}$)	Micropore area ($m^2 g^{-1}$)	External surface area ($m^2 g^{-1}$)	Pore volume ($cm^3 g^{-1}$)
Spray Si	117.69	82.93	34.76	0.152
Spray Si-Cu	109.57	70.01	39.56	0.176

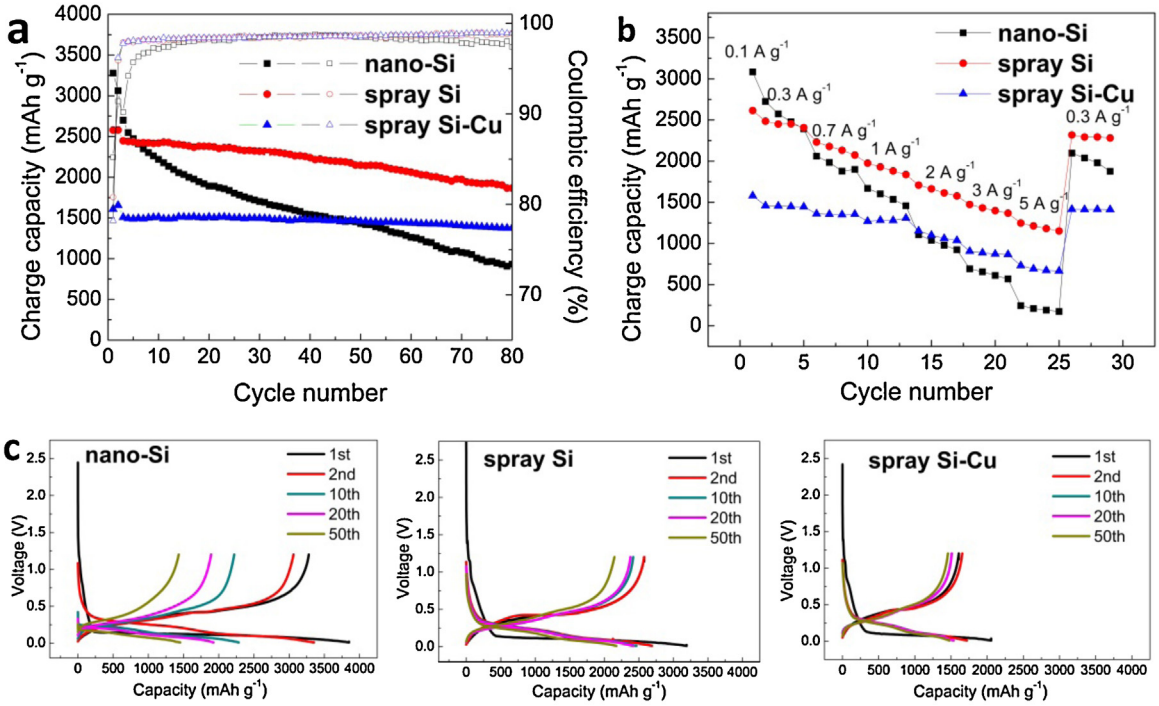

Fig. 8. (a) Cycling performance and coulombic efficiencies of spray Si, spray Si-Cu and nano-Si electrodes at a current rate of 0.1 A g^{-1} in the initial two cycles and at 0.3 A g^{-1} in the following cycles. (b) Reversible capacities of the nano-Si, spray Si and spray Si-Cu electrodes at different rates from 0.1 A g^{-1} to 5 A g^{-1}. (c) Galvanostatic charge-discharge profiles of three electrodes at current rate of 0.1 A g^{-1} in the initial two cycles and of 0.3 A g^{-1} in the following cycles.

high current rate of 5 A g^{-1}, against less than 250 mA h g^{-1} for nano-Si at the same condition. Similarly, spray Si-Cu can retain more than 50% capacity at 5 A g^{-1} compared to that at 0.3 A g^{-1}, which is much higher than that of nano-Si (ca. 10%). The large surface area and good electronic conductive network are responsible for the fast electrode kinetics.

Fig. 9 shows the impedance changes of spray Si and spray Si-Cu during cycling. All cells were tested after charging to 1.2 V. The depressed semicircle in the high-middle frequency region mainly corresponds to the charge transfer resistance (R_{ct}), and an oblique straight line in the low frequency region relates to the ion diffusion kinetics [26]. Compared to the first cycle, R_{ct} of both cells in 10th cycle declined, which indicates the initial cycling results in effective electrode activation. After 50 cycles, R_{ct} raised remarkably for spray Si, while the value of R_{ct} for spray Si-Cu stayed the same with the 1st cycle. It means that Cu modification can significantly stabilize the interface property due to its advantages in reinforcing the composite structure and improving electronic conductivity.

The electrode morphology and its evolution during cycling was examined by SEM. Fig. 10a and Fig. 10c show that the electrode fabrication process did not affect the particle morphology of both samples and the original spherical structures were maintained. After 150 cycles, silicon particles become larger because of the irreversible volume expansion for lithium insertion [18]. However, the microspheres of spray Si appear to expand with enlarged pores or even become loose (Fig. 10b). This change indicates that the mechanical strength of spray Si was not high enough to endure the volume change during long-term cycles at a high current rate of 1 A g^{-1}. In contrast, relatively stable and dense particle morphology can be maintained for spray Si-Cu (Fig. 10d). Its better structural steadiness against the repeated lithiation/delithiation process is confirmed.

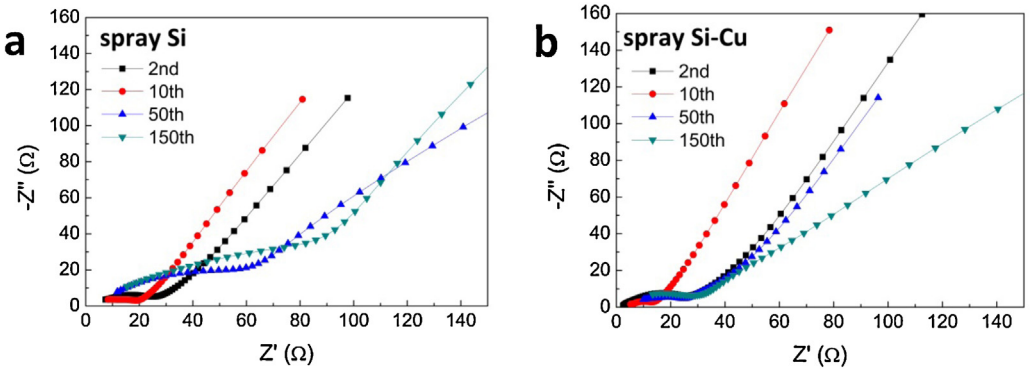

Fig. 9. Nyquist plots of the spray Si (a) and spray Si-Cu (b) electrodes during cycling at a current density of 1.0 A g^{-1}.

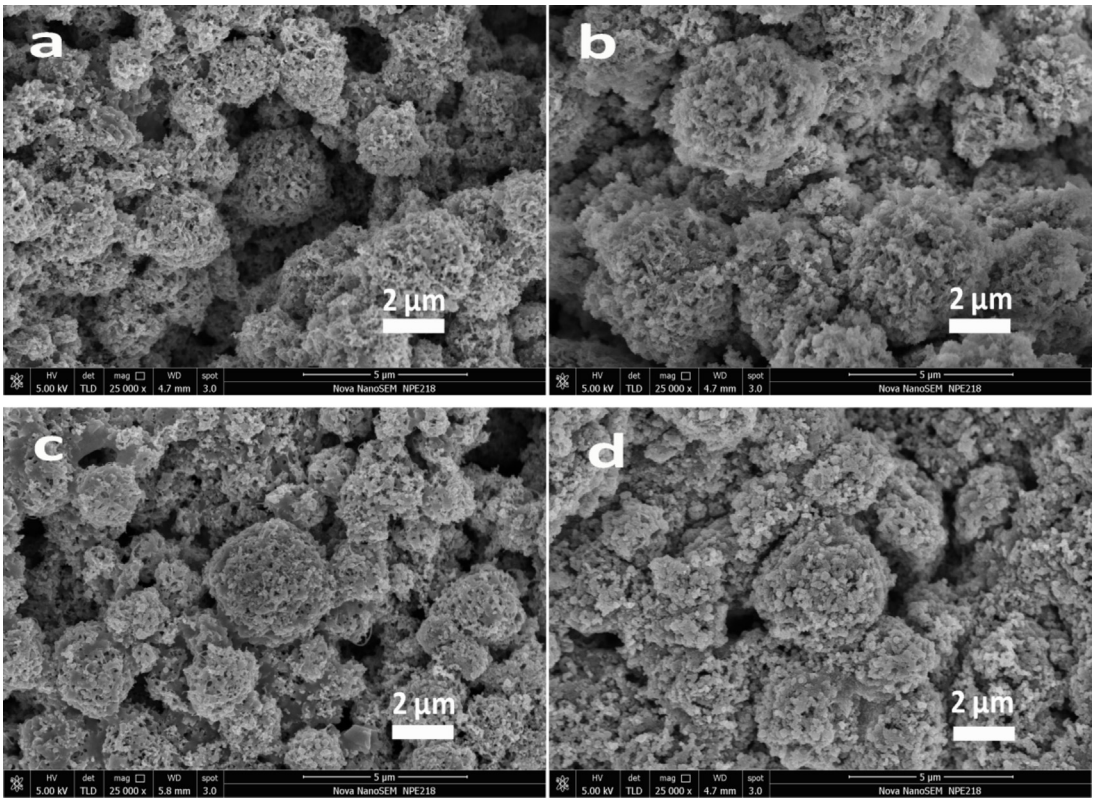

Fig. 10. SEM images of spray Si electrodes before cycling (a) and after 150 cycles (b), and spray Si-Cu electrodes before cycling (c) and after 150 cycles (d) at a current density of 1.0 A g^{-1}.

4. Conclusions

In summary, we have designed a facial approach to prepare microspherical silicon composite anode material. The whole process is based on simple, efficient and industrially established spray drying and high temperature carbonization. The obtained porous Si/CNT/C microspheres showed superior cycleability and rate performance with the specific capacity of 1248 mA h g^{-1} at a high current rate of 5 A g^{-1}. Moreover, the addition of copper led to nano-dispersion of Cu_3Si alloy in the porous microspheres, which reinforced the composite structure and enhanced the electrical conductivity. As a result, the porous Si-Cu/CNT/C composite possessed not only excellent cycle stability with capacity retention of 91.2% after 80 cycles, but also fast electrode kinetics. More than 50% capacity can be retained at 5 A g^{-1} compared to at 0.3 A g^{-1}.

Acknowledgement

This work was supported by State Key Basic Research Program of China (no. 2014CB932303) and SJTU-UM Joint Research Project.

References

[1] S. Sim, P. Oh, S. Park, J. Cho, Critical Thickness of SiO2Coating Layer on Core@Shell Bulk@Nanowire Si Anode Materials for Li-Ion Batteries, Adv Mater 25 (2013) 4498–4503.
[2] H. Wu, Y. Cui, Designing nanostructured Si anodes for high energy lithium ion batteries, Nano Today 7 (2012) 414–429.
[3] N.S. Choi, Z.H. Chen, S.A. Freunberger, X.L. Ji, Y.K. Sun, K. Amine, G. Yushin, L.F. Nazar, J. Cho, P.G. Bruce, Challenges Facing Lithium Batteries and Electrical Double-Layer Capacitors, Angew Chem Int Edit 51 (2012) 9994–10024.
[4] M. Ge, X. Fang, J. Rong, C. Zhou, Review of porous silicon preparation and its application for lithium-ion battery anodes, Nanotechnology 24 (2013) .
[5] S. Iwamura, H. Nishihara, T. Kyotani, Fast and reversible lithium storage in a wrinkled structure formed from Si nanoparticles during lithiation/delithiation cycling, J Power Sources 222 (2013) 400–409.
[6] W. Wang, P.N. Kumta, Nanostructured Hybrid Silicon/Carbon Nanotube Heterostructures: Reversible High-Capacity Lithium-Ion Anodes, Acs Nano 4 (2010) 2233–2241.
[7] C.K. Chan, R. Ruffo, S.S. Hong, Y. Cui, Surface chemistry and morphology of the solid electrolyte interphase on silicon nanowire lithium-ion battery anodes, J Power Sources 189 (2009) 1132–1140.
[8] M. Ge, J. Rong, X. Fang, C. Zhou, Porous Doped Silicon Nanowires for Lithium Ion Battery Anode with Long Cycle Life, Nano Lett 12 (2012) 2318–2323.
[9] H. Kim, J. Cho, Superior Lithium Electroactive Mesoporous Si@Carbon Core-Shell Nanowires for Lithium Battery Anode Material, Nano Lett 8 (2008) 3688–3691.
[10] D.S. Jung, T.H. Hwang, S.B. Park, J.W. Choi, Spray Drying Method for Large-Scale and High-Performance Silicon Negative Electrodes in Li-Ion Batteries, Nano Lett 13 (2013) 2092–2097.
[11] L. Hu, H. Wu, S.S. Hong, L. Cui, J.R. McDonough, S. Bohy, Y. Cui, Si nanoparticle-decorated Si nanowire networks for Li-ion battery anodes, Chem Commun 47 (2011) 367–369.
[12] B.M. Bang, J.-I. Lee, H. Kim, J. Cho, S. Park, High-Performance Macroporous Bulk Silicon Anodes Synthesized by Template-Free Chemical Etching, Adv Energy Mater 2 (2012) 878–883.
[13] W. Wang, P.N. Kumta, Reversible high capacity nanocomposite anodes of Si/C/SWNTs for rechargeable Li-ion batteries, J Power Sources 172 (2007) 650–658.
[14] X.M. Liu, Z.D. Huang, S.W. Oh, B. Zhang, P.C. Ma, M.M.F. Yuen, J.K. Kim, Carbon nanotube (CNT)-based composites as electrode material for rechargeable Li-ion batteries: A review, Compos Sci Technol 72 (2012) 121–144.
[15] X.L. Chen, X.L. Li, F. Ding, W. Xu, J. Xiao, Y.L. Cao, P. Meduri, J. Liu, G.L. Graff, J.G. Zhang, Conductive Rigid Skeleton Supported Silicon as High-Performance Li-Ion Battery Anodes, Nano Lett 12 (2012) 4124–4130.
[16] L.G. Xue, G.J. Xu, Y. Li, S.L. Li, K. Fu, Q. Shi, X.W. Zhang, Carbon-Coated Si Nanoparticles Dispersed in Carbon Nanotube Networks As Anode Material for Lithium-Ion Batteries, Acs Appl Mater Inter 5 (2013) 21–25.
[17] L.Y. Shao, J. Shu, K.Q. Wu, X.T. Lin, P. Li, M. Shui, D.J. Wang, N.B. Long, Y.L. Ren, Low pressure preparation of spherical Si@C@CNT@C anode material for lithium-ion batteries, Journal of Electroanalytical Chemistry 727 (2014) 8–12.
[18] X. Feng, J. Yang, Y. Bie, J. Wang, Y. Nuli, W. Lu, Nano/micro-structured Si/CNT/C composite from nano-SiO2 for high power lithium ion batteries, Nanoscale 6 (2014) 12532–12539.

[19] C. de las Casas, W.Z. Li, A review of application of carbon nanotubes for lithium ion battery anode material, J Power Sources 208 (2012) 74–85.
[20] C. Martin, O. Crosnier, R. Retoux, D. Belanger, D.M. Schleich, T. Brousse, Chemical Coupling of Carbon Nanotubes and Silicon Nanoparticles for Improved Negative Electrode Performance in Lithium-Ion Batteries, Advanced Functional Materials 21 (2011) 3524–3530.
[21] G.W. Zhou, J.L. Wang, P.F. Gao, X.W. Yang, Y.S. He, X.Z. Liao, J. Yang, Z.F. Ma, Facile Spray Drying Route for the Three-Dimensional Graphene-Encapsulated Fe2O3 Nanoparticles for Lithium Ion Battery Anodes, Ind Eng Chem Res 52 (2013) 1197–1204.
[22] S. Yoon, S.I. Lee, H. Kim, H.J. Sohn, Enhancement of capacity of carbon-coated Si-Cu3Si composite anode using metal-organic compound for lithium-ion batteries, J Power Sources 161 (2006) 1319–1323.
[23] H. Cai, D.B. Tong, Y.P. Wang, X.P. Song, B.J. Ding, Reactive synthesis of porous Cu3Si compound, J Alloy Compd 509 (2011) 1672–1676.
[24] J. Cho, Porous Si anode materials for lithium rechargeable batteries, Journal of Materials Chemistry 20 (2010) 4009–4014.
[25] J.H. Kim, H. Kim, H.J. Sohn, Addition of Cu for carbon coated Si-based composites as anode materials for lithium-ion batteries, Electrochemistry Communications 7 (2005) 557–561.
[26] J. Guo, A. Sun, X. Chen, C. Wang, A. Manivannan, Cyclability study of silicon–carbon composite anodes for lithium-ion batteries using electrochemical impedance spectroscopy, Electrochim Acta 56 (2011) 3981–3987.